THE JOURNAL OF PHYSICAL CHEMISTRY C

Article

Cite This: J. Phys. Chem. C 2019, 123, 2882−2893

pubs.acs.org/JPCC

Total Oxidation of Methane over Pt/Cr_2O_3 Catalyst at Low Temperature: Effect of Pt^0-Pt^{x+} Dipoles at the Metal−Support Interface

Grisel Corro*

Instituto de Ciencias, Benemérita Universidad Autónoma de Puebla, 4 sur 104, 72000 Puebla, México

Rosalía Torralba

Instituto de Ciencias, Benemérita Universidad Autónoma de Puebla, 4 sur 104, 72000 Puebla, México

Umapada Pal

Instituto de Física, Benemérita Universidad Autónoma de Puebla, Apdo. Postal J-48, 72570 Puebla, México

Octavio Olivares-Xometl

Facultad de Ingeniería Química, Benemérita Universidad Autónoma de Puebla, 4 sur 104, 72000 Puebla, México

José Luis G. Fierro

Instituto de Catálisis y Petroleoquímica, Cantoblanco, 28049 Madrid, España

Supporting Information

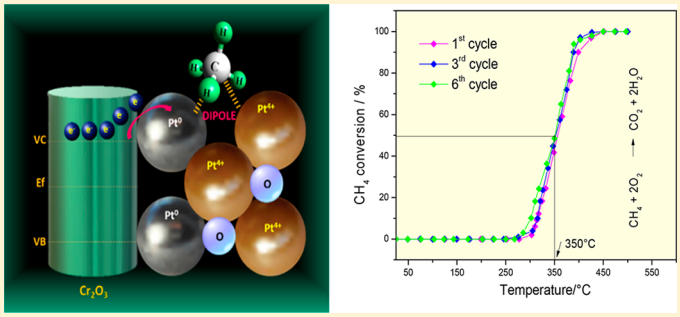

ABSTRACT: Catalytic activities of 1% Pt/Cr_2O_3 and 1% Pt/γ-Al_2O_3 have been studied in total methane oxidation under lean conditions. The catalysts were characterized by DRS, XPS, and HRTEM. Low-conversion catalytic tests performed at 310 °C revealed a TOF (h^{-1}) value 28 times larger for 1% Pt/Cr_2O_3 in comparison with 1% Pt/γ-Al_2O_3. The difference in TOF (h^{-1}) and the differences in T_{50} observed through the light-off curves (352 °C on 1% Pt/Cr_2O_3 and 460 °C on 1% Pt/γ-Al_2O_3) are explained on the basis of strong differences in the methane oxidation rate dependences of the pre-exponential factor in the Arrhenius type equations. XPS analysis of 1% Pt/Cr_2O_3 revealed the presence of stable Pt^0-Pt^{4+} catalytic sites of dipolar nature at the Pt/Cr_2O_3 interface. These sites are capable of increasing the probability of CH_4 polarization, resulting in an increase of the strength and oriented collisions between the molecules and the catalyst surface, lowering the C−H bond energy, facilitating the abstraction of the first hydrogen in the adsorbed methane: the rate-determining step of methane oxidation. The high stability of the Pt^0-Pt^{4+} sites has been associated with the electronic interactions between platinum and n-type semiconductor Cr_2O_3 at their interface.

1. INTRODUCTION

To restrict the emission of greenhouse gases, sustainable automotive transports are required. In this regard, the lean-burn gas engines provide an important alternative to conven-

Received: October 5, 2018
Revised: January 10, 2019
Published: January 14, 2019

DOI: 10.1021/acs.jpcc.8b09748
J. Phys. Chem. C 2019, 123, 2882−2893

tional diesel or gasoline engines, due to their efficiency, low-temperature fuel combustion under excess oxygen, and the utilization of natural gas and biogas. The use of methane in energy conversion processes is expected to increase in coming years due to its high abundance as natural gas. Additionally, methane (CH_4) can also be produced from biological feedstocks in the form of biogas.[1−4] Natural gas and biogas are considered attractive combustion fuels because they contain low levels of nitrogen and sulfur related pollutants and the amount of formed CO_2 per produced quantity of combustion heat is relatively low.[5,6]

Natural gas and biogas essentially consist of methane, which is the most stable hydrocarbon. The complete oxidation of methane follows the reaction

$$CH_4 + 2O_2 \rightarrow CO_2 + 2H_2O$$

which is strongly exothermic, having $\Delta H_{rxn} = -891$ kJ/mol.[7] However, the reaction has a substantial activation energy. The abstraction of the first H atom, commonly considered as the limiting step, requires 430 kJ/mol.[8] While the reaction is spontaneous at 1000 °C,[9] the temperature can be reduced substantially by the use of an oxidation catalyst.

As has been mentioned earlier, the emission of CH_4 (a strong greenhouse gas) is the main hindrance for the utilization of natural gas or biogas as fuel. For reducing the emission of such greenhouse gases, gas engine generators are frequently coupled with integrated after-treatment options such as selective catalytic reduction (SCR) and oxidation catalysts. However, the main challenge for that is to find suitable catalysts, which can ensure a total oxidation of CH_4 in lean and cold exhausts at acceptable rates, for a prolonged period.

Several metals such as platinum,[10−16] palladium,[17−19] and copper[20] or their combinations[21−24] have been studied as methane oxidation catalysts, with palladium recognized as the most active.[1,25,26] However, Pd-based catalysts are sensitive toward sulfur poisoning. Even a small amount of sulfur containing species in the exhaust can deactivate such catalysts due to the formation of stable palladium sulfates.[27,28] On the other hand, Pt is known to be one of the most active metals for hydrocarbon oxidation, with activity comparable to Pd. Moreover, platinum is more sulfur tolerant than palladium,[27,29] although its methane oxidation activity strongly depends on the composition of the reactant gas mixture. For example, the oxidation of methane over Pt/Al_2O_3 is inhibited under oxygen excess.[27−35]

In the kinetic regime, methane oxidation is limited by the dissociative adsorption of methane.[36] On the other hand, the sticking probability of methane on noble metal surfaces is low.[37] In addition, its dissociation strongly depends on the surface coverage of reaction intermediates. In general, the oxidation process of methane is seen to follow the Mars−van Krevelen reduction−oxidation pathways,[38] where the rate-determining step is the abstraction of the first hydrogen on adsorbed methane molecule and the oxygen chemisorption steps are not kinetically significant.[15,39] Burch et al. speculated the possibility of a more efficient activation of the C−H bond for dissociation via heterolytic splitting, through the polarization of CH_4 molecule by platinum surface, covered partially by oxygen.[36] On the other hand, a higher methane oxidation rate over the Pt[111]-(2 × 2)-O surface compared with the Pt[111] surface has been noted by Kondo et al.[40] A few years later, Beck et al. observed that the total oxidation of methane over 1% Pt/γ-Al_2O_3 catalyst depends strongly on the size of Pt nanoparticles, obtaining a bell-shaped turnover frequency (TOF) versus mean size curve for the supported particles.[41] While the maximum TOF was observed for the Pt particles of ∼2 nm average size, the catalyst contained comparable amounts of partially oxidized and metallic platinum species. Although the high activity of those Pt-supported catalysts has been associated with different parameters like the size of Pt particles, specific crystallographic planes, etc., the results clearly indicate a probable activation of the C−H bond over the platinum surface containing Pt^0-Pt^{x+} sites, which can polarize the CH_4 molecule, decreasing the C−H bond energy and facilitating its cleavage.

In the present work, we investigate the possibility of developing such dipolar catalytic sites to improve the methane dissociation and thus the methane oxidation activity of Pt supported metal oxide catalysts. As the electron transfer process between the supported metal and supporting metal oxide is known to play an important role in the production of metal ions of different valence states, and hence on the catalytic activity of supported catalysts,[42] we analyzed the valence state of platinum supported on n-type semiconductor Cr_2O_3, to correlate the effect of the support on the development of stable and active Pt^0-Pt^{x+} polar sites, on the catalytic activity of Pt-supported Cr_2O_3 on the total oxidation of methane. The structural and electronic properties of the catalysts were studied using X-ray photoelectron spectroscopy (XPS), UV−vis diffuse reflectance spectroscopy (DRS), and high-resolution transmission electronic microscopy (HR-TEM). The catalytic behavior of the composites in methane oxidation in the 25−500 °C temperature range has been correlated with its physicochemical properties, considering the interactions of active and nonactive species such as Pt^0, Pt^{2+}, and Pt^{4+} with oxygen and CH_4, along with the interactions between platinum and the Cr_2O_3 support.

2. EXPERIMENTAL SECTION

2.1. Catalyst Preparation. Commercial Cr_2O_3 powder (Sigma-Aldrich, 99.99%, particle size: retained by 50 μm sieve) and γ-Al_2O_3 powder (Merck 99.99%, particle size: 0.063−0.200 mm) were used to prepare Pt supported catalysts. The catalysts were prepared by impregnating Cr_2O_3 or γ-Al_2O_3 powder with an aqueous solution of platinum hexachloride ($H_2PtCl_6{\cdot}6H_2O$, Aldrich, 99.99%) of appropriate concentration to obtain nominal 1 wt % Pt/metal-oxide mixtures. The suspension was magnetically stirred at room temperature for 1 h; afterward, the catalyst was recovered by filtration and washed thoroughly to remove chlorine, and other unreacted species (if any), dried at 120 °C overnight, and calcined under air flow (100 mL min^{-1}) in a tubular furnace at 600 °C for 4 h. A linear heating ramp of 10 °C min^{-1} was utilized to reach the maximum temperature. After cooling down to room temperature, the catalysts, designated as 1% Pt/Cr_2O_3 and 1% Pt/γ-Al_2O_3, were stored under dry conditions. Cr_2O_3 and γ-Al_2O_3 samples without platinum ion impregnation were prepared in the same way to serve as the references.

2.2. Catalyst Characterization. A Belsorp Mini II sorptometer was used to measure the N_2 adsorption−desorption isotherms of the catalysts. The specific surface area (S_g) of the samples was estimated from their N_2 physisorptions at 77 K, using BET analysis. The samples (0.5 g each) were degassed at 400 °C for 2 h before recording their adsorption−desorption isotherms. After cooling to room temperature (25 °C), the isotherms were recorded in the pressure range 0.0−6.6 kPa. The technique of back extrapolation of the linear portion of

DOI: 10.1021/acs.jpcc.8b09748
J. Phys. Chem. C 2019, 123, 2882−2893

the isotherms to zero equilibrium pressure was used to determine the saturation uptake.

The diffuse reflectance spectra (DRS) of the catalysts before and after six methane oxidation cycles were measured on dry-pressed disks (~15 mm diameter) using a Shimadzu UV−vis spectrophotometer equipped with an integrating sphere and $BaSO_4$ as a standard reflectance sample. The crystallinity and structural phase of the samples were verified through powder X-ray diffraction (XRD), using the Cu Kα radiation (λ = 1.5406 Å) of a Bruker D8 Discover diffractometer.

The X-ray photoelectron spectra (XPS) were recorded on the catalysts before and after six methane oxidation cycles, using an Escalab 200R electron spectrometer equipped with a hemispherical analyzer, operating in a constant pass energy mode. Monochromatic Mg Kα emission ($h\nu$ = 1253.6 eV) from the X-ray tube operating at 10 mA and 12 kV was utilized for recording XPS spectra of the samples. Different energy regions of interest of the photoelectrons were scanned a number of times in order to get good signal-to-noise ratios. The intensities of the emission peaks were estimated by determining the integral of each peak after subtracting an S-shaped background and fitting the experimental peak to Lorentzian/Gaussian curves (80% L/20% G). The peak positions of the elements were corrected utilizing the position of the C 1s peak coming from adventitious carbon that appeared at 284.9 ± 0.2 eV.

High-resolution transmission electron microscopic (HR-TEM) images of the 1% Pt/Cr_2O_3 catalysts before and after six methane oxidation cycles were obtained in a JEM-ARM200CF, JEOL, microscope (lattice resolution 78 pm, acceleration voltage 200 kV). The samples for microscopic observations were prepared by dispersing the powder catalysts in ethanol and drop casting on carbon coated copper grids. The size distribution histogram of the platinum nanoparticles was prepared by measuring the size of 150−200 particles for each sample.

Assuming a spherical shape of the formed Pt nanoparticles, their mean size (d_{Pt}) was calculated using eq 1

$$d_{Pt} = \Sigma V_i / \Sigma S_i \text{ (nm)} \quad (1)$$

where V_i and S_i are the volume and surface area of the ith particle, respectively.

The Pt dispersion value D_{Pt} is defined as shown in eq 2

$$D_{Pt} = \frac{\text{Number of surface Pt atoms}}{\text{Number of Pt atoms}} \quad (2)$$

For 1% Pt/Cr_2O_3 and 1% Pt/γ-Al_2O_3, the number of Pt atoms per gram of catalyst was about 3.08×10^{19}.

The number of surface Pt atoms was calculated assuming that the dispersion value D_{Pt} can be calculated from the surface area and mean Pt particle size according to eq 3[43]

$$D_{Pt} = 6 \cdot V_{Pt} / a_{Pt} \cdot d_{Pt} \quad (3)$$

where V_{Pt} = Pt atomic volume and a_{Pt} = average surface area occupied by one Pt atom.

The values of V_{Pt} and a_{Pt} were calculated as

$$V_{Pt} = M_{Pt} \cdot \frac{10^{21}}{\rho} \cdot N_A = 0.015 \text{ nm}^3$$

$$a_{Pt} = 1 \times 10^{14} / \sigma = 0.08 \text{ nm}^2$$

where M_{Pt} = Pt molecular mass (195.05 g mol^{-1}), ρ = density of Pt (21.45 g cm^{-3}), N_A = the Avogadro number (6.023×10^{23} atoms mol^{-1}), and σ = the concentration of the Pt atoms on the metallic surface (1.25×10^{15} cm^{-2}).

2.3. Catalytic Tests. All of the catalytic tests were performed at 1 atm, in a continuous flow tubular quartz reactor of 10 mm inner diameter, placed inside a programmable furnace with internally mounted thermocouple. Reactant gases were fed from independent mass flow controllers. Methane oxidation tests over the catalysts were performed under a 100 cm^3 min^{-1} flow rate of feed gas, constituting 0.2 vol % CH_4, 10 vol % O_2, and balance N_2. The catalyst loading (W) in the reactor was 200 mg diluted with 1 g of low surface area quartz (<1 m^2 g^{-1}) to prevent heat transfer limitations, and the contact time (W/F^0) was 373 g of catalyst h/mol of CH_4. The reactor outflow was analyzed in a Shimadzu gas chromatograph, provided with a thermoconductivity detector (TCD).

Two experimental procedures were used for testing the catalysts. Before performing the experimental tests, the samples were pretreated in the reactant stream at 600 °C for 1 h. Afterward, they were cooled down (keeping in the reactant stream) to 25 °C.

The total CH_4 oxidation was studied by following the evolution of methane conversion as a function of temperature (light-off curves). Catalytic oxidation of CH_4 (methane conversion) was performed in the 25−600 °C temperature range, heating the catalysts at 2 °C min^{-1}. The samples were then cooled down again to 25 °C. The process comprising the methane oxidation from 25 to 600 °C is defined as a cycle. Although the catalysts were heated at 2 °C min^{-1}, sufficient time was allowed at each of the measurement temperatures to reach a steady state. To verify the long-term resistivity of the catalysts, six similar cycles were performed over the same catalyst sample. Temperature-programmed reaction profiles allowed us to determine the temperature at which methane conversion attains 10% (T_{10}), 50% (T_{50}), and 100% (T_{100}).

The fundamental differential reactor experiments were performed at constant temperature. Arrhenius parameters were calculated for below 10% conversion to avoid diffusion limitations. The presence of water in the products was verified without quantification. Carbon monoxide was never detected in the effluent.

3. RESULTS AND DISCUSSION

3.1. Catalyst Characterization. *3.1.1. Surface Area Analysis.* The specific surface area of the catalysts before utilization in oxidation cycles was estimated from their N_2 adsorption−desorption isotherms recorded at 77 K. The obtained results are summarized in Table 1. It can be seen in the table that the values did not change much after their use in oxidation cycles.

The mean size of Pt particles d_{Pt}, the values of dispersion D_{Pt}, and the number of surface Pt atoms g·cat^{-1}, were calculated using eqs 1, 2, and 3 for the fresh catalyst, as summarized in Table 1.

3.1.2. UV−vis Characterization of the Catalysts. Figure 1 shows the optical absorption spectra of Cr_2O_3 and 1% Pt/Cr_2O_3 catalysts before and after six methane oxidation cycles, measured in diffuse reflectance mode in the UV−vis spectral range. The absorption spectra of Cr_2O_3 and 1% Pt/Cr_2O_3 are dominated by four bands. The absorption bands centered on 250 and 370 nm are usually assigned to the transitions associated with charge transfer from O^{2-} to Cr^{6+} of the tetrahedrally coordinated Cr^{6+} and indicate the presence of highly isolated Cr^{6+} ions.[44−47] The band that appeared around 460 nm is characteristic of Cr^{6+}

DOI: 10.1021/acs.jpcc.8b09748
J. Phys. Chem. C 2019, 123, 2882−2893

Table 1. Characteristics of Samples Used in This Study[a]

catalyst	specific surface area ($m^2\ g^{-1}$) fresh sample	specific surface area ($m^2\ g^{-1}$) after oxidation cycles	D_{Pt} fresh sample	d_{Pt} (nm)	number of surface Pt atoms ($g^{-1} \times 10^{19}$) fresh sample
Cr_2O_3	6.1	5.4			
1% Pt/Cr_2O_3	5.2	5.2	0.93	1.18	2.61
γ-Al_2O_3	310	300			
1% Pt/γ-Al_2O_3	280	265	0.37	3.0	1.15

[a]The dispersion values were calculated from TEM data. The number of surface Pt atoms in the catalyst was calculated from dispersion values, considering 3.08×10^{19} Pt total atoms/g of catalyst.

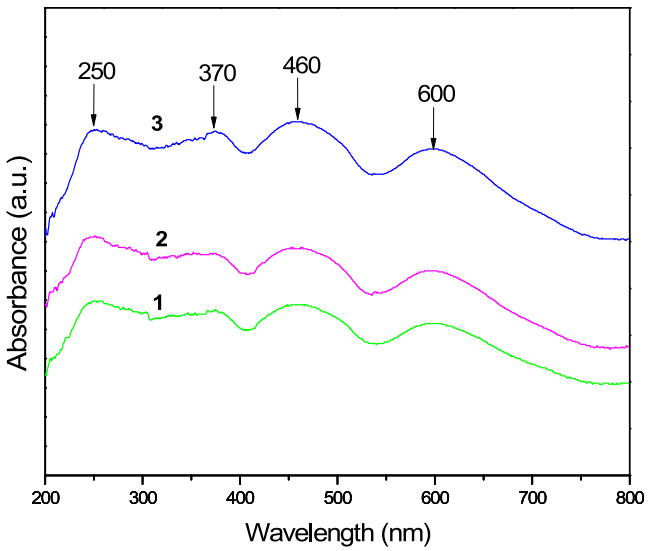

Figure 1. Absorption spectra of (1) Cr_2O_3, (2) 1% Pt/Cr_2O_3 before methane oxidation cycles, and (3) 1% Pt/Cr_2O_3 after methane oxidation cycles.

polychromate $(-Cr-O-Cr-)n$ in the framework. The strong absorption band spanning 550–750 nm corresponds to the octahedral Cr^{3+} species in the catalyst.[48] It is interesting to note the similarities between the spectra of the catalysts containing Pt and without Pt. Such results are expected, as Pt nanoparticles, in 1% Pt/Cr_2O_3, with an average size of ~1.18 ± 0.35 nm (Table 2) do not show discrete surface plasmon absorptions in the visible spectrum because of a damping effect caused by the d–d interband transition (the plasmon energy is lost by excitation of single electron interband transitions).[49,50] In fact, severe plasmon damping generally occurs for the noble metal nanoparticles when their size becomes lower than 2 nm.[51]

As can be seen in Figure 1, the absorption spectrum of 1% Pt/Cr_2O_3 catalyst after its use in oxidation cycles (spectrum 3) revealed the same absorption bands as the catalyst before use in methane oxidation cycles (spectrum 2). The results suggest that the same electronic states of the catalyst components prevail in 1% Pt/Cr_2O_3 even after six methane oxidation cycles.

The UV–vis diffuse reflectance spectra (DRS) of γ-Al_2O_3 and 1% Pt/γ-Al_2O_3 before and after their use in methane oxidation cycles are represented in Figure 2.

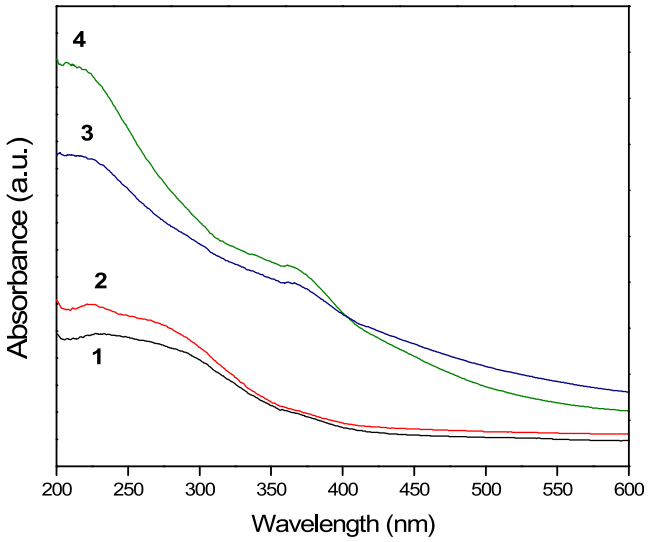

Figure 2. Absorption spectra of (1) γ-Al_2O_3 before methane oxidation cycles, (2) γ-Al_2O_3 after methane oxidation cycles, (3) 1% Pt/γ-Al_2O_3 before methane oxidation cycles, and (4) 1% Pt/γ-Al_2O_3 after methane oxidation cycles.

The absorption spectra of 1% Pt/γ-Al_2O_3 present an intense absorption at high energy spreading between 200 and 300 nm which has been assigned to charge transfer from chloride ligands to platinum in oxychloride surface complexes $[PtO_xCl_y]$.[52–54] The band spreading between 325 and 400 nm can be attributed to d–d transitions in bulk compounds such as $PtO_x \cdot H_2O$.[52–54] As can be noticed (Figure 2), the plasmon damping did not occur in the 1% Pt/Al_2O_3 sample. The result was expected, as the Pt nanoparticles in 1% Pt/Al_2O_3 with an average size of ~3.0 ± 0.35 nm (Table 2) manifest discrete surface plasmon absorptions in the visible region of the spectrum.[51]

As can be seen, there is hardly any difference between the absorption spectra of the catalyst recorded before (spectrum 3) and after methane oxidation (spectrum 4). This result suggests that the electronic state of Pt particles in 1% Pt/γ-Al_2O_3 remained the same, even after six methane oxidation cycles.

3.1.3. XPS Characterization of the Catalysts. 1% Pt/Cr_2O_3. The catalytic performance of a material in oxidation reaction is frequently correlated with its capability to activate oxygen. To determine the possible interactions between the catalyst and oxygen, electronic properties of Cr_2O_3 and 1% Pt/Cr_2O_3 were studied by XPS (Figure 3). Estimated binding energy (BE) values of Pt $4f_{7/2}$ and Cr $2p_{3/2}$ levels and atomic percentages of Pt species in different oxidation states are presented in Table 3.

Table 2. Methane Oxidation Rates Measured from Low-Conversion Catalytic Tests (T = 310°C, P = 1 atm, $CH_4/O_2/N_2$ = 0.2/10/89.8; 5.35×10^{-4} mol of CH_4/h)

catalyst	d_{Pt} (nm)	number of surface Pt atoms/g of catalyst	number of surface Pt atoms/g of Pt	r_0 (mol of CH_4/h g of Pt)	TOF (h^{-1})
1% Pt/Cr_2O_3	1.2	2.64×10^{19}	2.64×10^{17}	0.0245	5.59
1% Pt/γ-Al_2O_3	3.0	1.15×10^{19}	1.15×10^{17}	0.0004	0.21

DOI: 10.1021/acs.jpcc.8b09748
J. Phys. Chem. C 2019, 123, 2882–2893

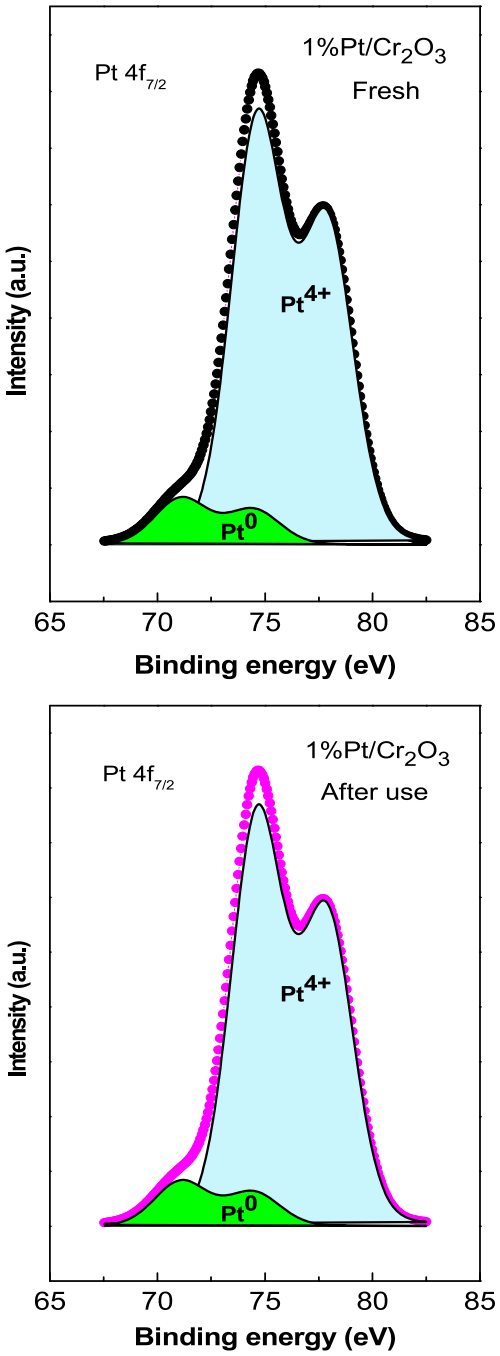

Figure 3. Pt $4f_{7/2}$ core level XPS spectra of freshly prepared 1% Pt/Cr_2O_3 and after its use in six methane oxidation cycles.

While the XPS spectrum of 1% Pt/Cr_2O_3 revealed a single component Cr $2p_{3/2}$ emission band located around 576.4 eV (Figure S1), which corresponds to the Cr^{3+} state,[55−57] the Pt $4f_{7/2}$ emission band revealed two components: a low intensity component located around 71.6 eV, associated with Pt^0, and a second one at 74.6 eV. This last component has been assigned to the Pt^{2+} state[58,59] or to Pt^{4+}.[60−62] Nevertheless, the peak width suggests a combination of Pt^{2+} and Pt^{4+}, since binding energy values are rather close and the spectral resolution of the spectrometer does not allow the components to be distinguished unequivocally. For giving more insight into these results, the XPS spectra of the Pt $4d_{5/2}$ band for the freshly prepared 1% Pt/Cr_2O_3 and after its use in methane oxidation are displayed in Figure S2. As can be seen, the Pt $4d_{5/2}$ emission band of the fresh catalyst after its use revealed a major signal located at 316.9 eV corresponding to Pt^{2+} and two minor components: one at 314.0 eV assigned to Pt^0 and the other one at 318.6 eV assigned to Pt^{4+}.[63,64] These results indicate the dominant presence of Pt^{2+}, with minor proportions of Pt^0 and Pt^{4+} species at the catalyst surface.

Table 3. Binding Energy Positions of the Components and Pt/Cr and Pt/Al Atomic Ratios at the Surface of the Catalysts before (Fresh) and after Using Them in Six Methane Oxidation Cycles (Used)[a]

catalyst	Pt $4f_{7/2}$ (eV)	Cr $2p_{3/2}$ (eV)	O 1s (eV)	Pt/Cr atomic ratio
1% Pt/Cr_2O_3 (fresh)	71.6 (10) 74.6 (90)	576.4	530.2	0.34
1% Pt/Cr_2O_3 (used)	71.6 (10) 74.6 (90)	576.4	530.3	0.34
	Pt $4d_{5/2}$ (eV)	Al 2p (eV)	O 1s (eV)	Pt/Al atomic ratio
1% Pt/γ-Al_2O_3 (fresh)	317.2 (100)	74.5	530.2	0.31
1% Pt/γ-Al_2O_3	317.2 (100)	74.5	530.3	0.32

[a]The % peak area of Pt^0, Pt^{2+}, and Pt^{4+} components is presented in parentheses.

The XPS estimated Pt/Cr ratio in the catalyst (Table 3) indicates about 30% of the Cr surface atoms are covered by platinum species, suggesting a high metallic dispersion in the sample. Such a high metallic dispersion indicates the formation of small metallic nanoparticles.

It is worth noting that, while XPS spectra revealed the presence of only Cr^{3+} species, the DRS spectra of Cr_2O_3 and of 1% Pt/Cr_2O_3 (Figure 1) revealed absorption bands associated with Cr^{3+} and Cr^{6+}, indicating the presence of both Cr species. These apparent contradictions between the DRS and XPS results can be justified considering that the DRS technique is a bulk technique, providing information on the entire sample, while the XPS technique is a surface technique, providing the surface composition of the catalyst up to a few nm depth, detecting the presence of only Cr^{3+} species at its surface.

1% Pt/γ-Al_2O_3. XPS analysis was carried out on the fresh 1% Pt/γ-Al_2O_3 catalysts and after their use in methane oxidation cycles. A common problem in the XPS study of 1% Pt/γ-Al_2O_3 catalysts is the fact that the Al 2p line of the support overlaps with the Pt 4f line of the active component, usually used for the spectroscopic analysis of platinum. This makes direct analysis of the platinum states very complicated. Therefore, in this study, we used the Pt 4d peaks, particularly the $4d_{5/2}$ peaks which are easily detected. Although this line is weaker, it is not overlapped with the spectral lines of other components.

XPS spectra of the Pt $4d_{5/2}$ band for the freshly prepared 1% Pt/γ-Al_2O_3 and after its use in methane oxidation are displayed in Figure 4. Estimated binding energy (BE) values of the Pt $4d_{5/2}$ level and atomic percentages of Pt species in different oxidation states are presented in Table 3. As can be seen, the Pt $4d_{5/2}$ emission band revealed a single binding energy component (317.2 eV) indicating that Pt is present only as Pt^{2+}.[56,65,66] The XPS estimated Pt/Al ratio in the catalyst (Table 3) indicates about 30% of the Al surface atoms are covered by platinum species, suggesting a high metallic dispersion in the sample. Such a high metallic dispersion indicates the formation of small metallic nanoparticles.

DOI: 10.1021/acs.jpcc.8b09748
J. Phys. Chem. C 2019, 123, 2882−2893

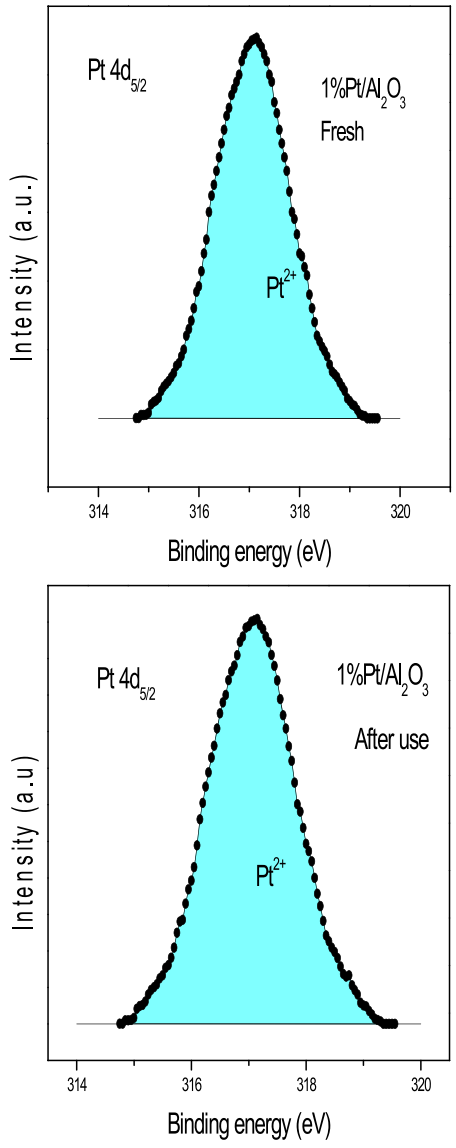

Figure 4. Pt $4d_{5/2}$ core level XPS spectra of the catalysts freshly prepared in 1% Pt/γ-Al_2O_3 and after its use in six methane oxidation cycles.

3.1.4. HR-TEM Analysis of the Catalyst. 1% Pt/Cr_2O_3. Typical HR-TEM images of the fresh Cr_2O_3 and 1% Pt/Cr_2O_3 samples are shown in Figure 5. Formation of small, highly dispersed Pt nanoparticles over the Cr_2O_3 surface can be seen (Figure 5b–d). The size of the formed Pt particles varied between 0.6 and 2.0 nm, with an average size of ~1.18 ± 0.35 nm. To justify the homogeneous distribution of uniform Pt nanoparticles over the catalyst, we presented several HR-TEM images of the sample in the Supporting Information (Figure S3). It is well-known that small metal nanoparticles can present electron deficiencies due to metal–support interactions,[67,68] in contrast to those of larger metal nanoparticles. This fact and the fact that the catalyst was calcined at 600 °C in air before its use in methane oxidation reactions explain the high content of relative Pt^{x+} species at the surface of Cr_2O_3, as revealed by the XPS analysis of the Pt-loaded catalyst. Notwithstanding, these facts do not explain the 10% content of metallic Pt^0 surface species present at the catalyst surface.

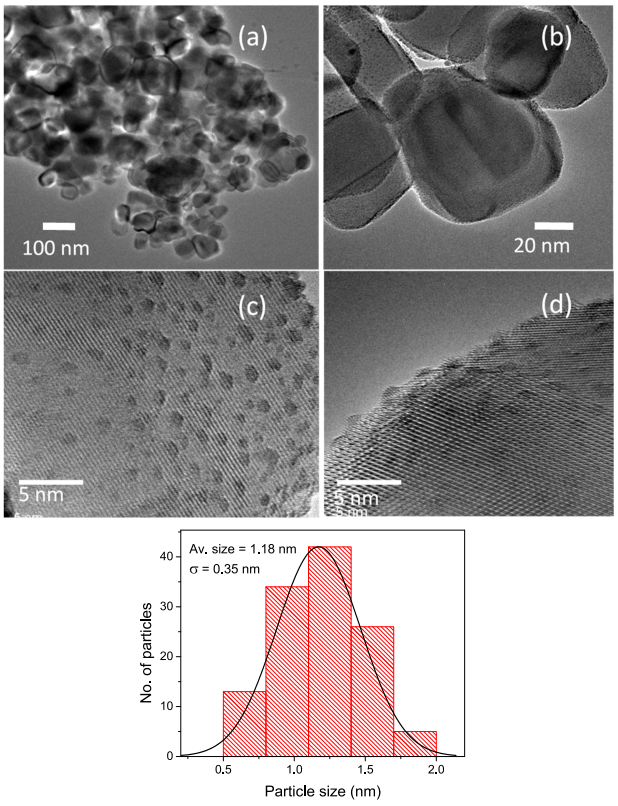

Figure 5. Typical TEM images of freshly prepared (a) Cr_2O_3 and (b) 1% Pt/Cr_2O_3 catalysts and (c, d) HRTEM images of 1% Pt/Cr_2O_3 catalyst. Formation of Pt nanoparticles of 0.6–2.0 nm range at the surface of Cr_2O_3 is very clear in the high-resolution images presented in parts c and d.

To explain the presence of fully reduced platinum (Pt^0) at the surface of the catalyst, we must consider the semiconducting nature of the Cr_2O_3 and the concept of energy level alignment between Pt nanoparticles and Cr_2O_3 support. As the work function of Pt (~6.9 eV) is quite a bit higher than that of Cr_2O_3 (~5.6 eV),[42] the formation of metallic Pt^0 at the catalyst surface might have been caused by the electron transfer from Cr_2O_3 to platinum nanoparticles during the formation of a Pt–Cr_2O_3 composite. The Fermi energy level of the electrons will migrate from Cr_2O_3 to the conduction band (CB) of Pt to achieve the Fermi level equilibration when they are in contact, decreasing the stability of Pt^{x+} at the metal–support interface.[69,70] The electron transfer from Cr_2O_3 to Pt results in the formation of Pt^0, as revealed by XPS analysis.

1% Pt/γ-Al_2O_3. A typical TEM image of the freshly prepared 1% Pt/γ-Al_2O_3 catalysts is presented in Figure 6. Formation of Pt nanoparticles in the 2.0–5.5 nm range with an average size of ~3 nm can be clearly observed from the micrograph. It can also be noticed that the Pt particles formed over an alumina support are not as monodispersed as the Pt nanoparticles formed over the chromia support (Figure 5). They revealed no well-arranged lattice planes in the TEM image of the composite catalyst due to the amorphous nature of alumina (Figure S4).

The results presented in Figures 5 and 6 and in Table 2 show the effect of two supports Cr_2O_3 and γ-Al_2O_3 on the size distribution of platinum particles. As can be noticed, the average size of the Pt nanoparticles formed over 1% Pt/γ-Al_2O_3 (~3 nm) is bigger than the one estimated for 1% Pt/Cr_2O_3 (~1.18 nm). As both of the samples were prepared and calcined under similar

DOI: 10.1021/acs.jpcc.8b09748
J. Phys. Chem. C 2019, 123, 2882–2893

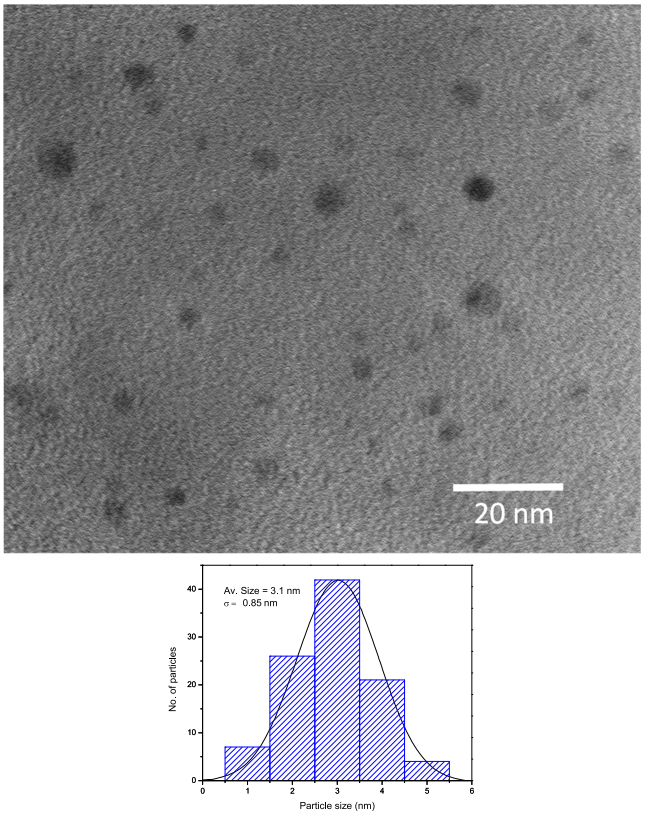

Figure 6. Typical TEM image of the freshly prepared 1% Pt/γ-Al_2O_3 catalysts.

experimental conditions, the difference in the size of Pt nanoparticles over the two supports might have occurred from the differences in their surface energy and the nature of chemical species attached to them.

3.2. Methane Oxidation over the Catalysts. *Light-off Curves over Cr_2O_3 and 1% Pt/Cr_2O_3.* In Figure 7, the evolutions of CH_4 conversion with reaction temperature during six oxidation cycles over 1% Pt/Cr_2O_3 are presented. As can be seen, Cr_2O_3 presents a very low activity for the reaction. The

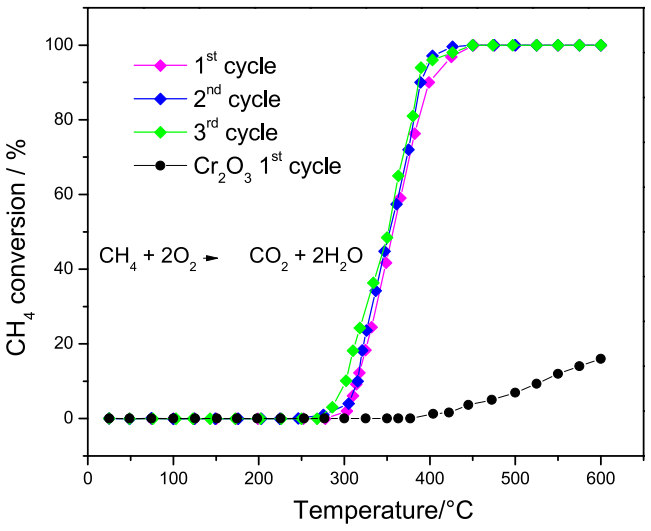

Figure 7. Methane conversion as a function of reaction temperature over 1% Pt/Cr_2O_3 and Cr_2O_3 catalysts.

values calculated from the curves led to the construction of Figure S5 (Supporting Information) which summarizes the T_{50} and T_{100} values obtained for the conversion of CH_4 on CH_4–O_2 reaction.

The percentage of CH_4 conversion in the 25–600 °C temperature range over Cr_2O_3 revealed very low methane conversion during the first and subsequent oxidation cycles. However, the conversion of CH_4 was substantially high for the 1% Pt/Cr_2O_3 composite catalyst. Moreover, the temperatures of 10% (T_{10}), 50% (T_{50}), and 100% (T_{100}) methane conversion over the catalyst remained almost the same until the sixth cycle (Figure 7 and Figure S5), indicating a very high stability of the catalysts for the reaction. The unaltered T_{10}, T_{50}, and T_{100} values also indicate the stoichiometry and electronic structure of the catalyst remained unaltered during the six oxidation cycles.

In Figure S6, the temperature of 100% methane conversion (T_{100}) as a function of reaction time over 1% Pt/Cr_2O_3 is presented. The figure shows that, after 8 h of reaction time, the T_{100} remained almost unaltered (440 ± 3 °C). The above result also suggests that the stoichiometry and electronic structure of the catalyst remain unchanged during 8 h of reaction, showing a high stability of the catalyst.

Light-off Curves over 1% Pt/γ-Al_2O_3. The percentage of CH_4 conversion in the 25–600 °C temperature range over γ-Al_2O_3 (results not shown) revealed very low methane conversion during the six methane oxidation cycles. The results obtained of the percentage of CH_4 conversion evolution with reaction temperature during six oxidation cycles over 1% Pt/γ-Al_2O_3 in the 25–600 °C temperature range are presented in Figure 8. As

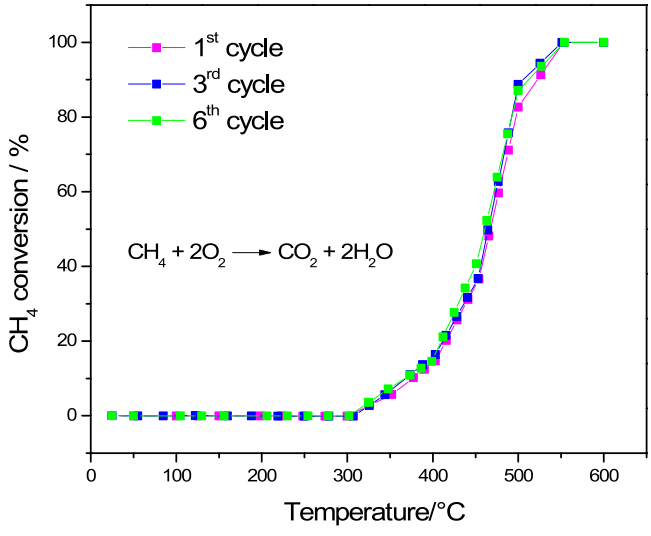

Figure 8. Methane conversion as a function of reaction temperature over 1% Pt/γ-Al_2O_3 catalyst.

can be seen, in the lower temperature range, the conversion of CH_4 is much lower for this catalyst compared with that of 1% Pt/Cr_2O_3. The temperatures of 10% (T_{10}), 50% (T_{50}), and 100% (T_{100}) methane conversion measured over 1% Pt/γ-Al_2O_3 catalyst are about 100 °C higher than those measured for 1% Pt/Cr_2O_3. On the other hand, the methane oxidation activity remained almost the same until the sixth cycle (Figure 8 and Figure S5) for both catalysts, indicating a high stability of the catalysts for this reaction.

Kinetic Studies over the Catalysts. Methane oxidation experiments were also performed over the platinum supported

DOI: 10.1021/acs.jpcc.8b09748
J. Phys. Chem. C 2019, 123, 2882–2893

catalysts at constant temperature between 260 and 310 °C and between 310 and 350 °C on 1% Pt/Cr_2O_3 and 1% Pt/γ-Al_2O_3, respectively. The initial conversions were lower than 10% in these temperature ranges. Figures S7 and S8 (Supporting Information) show the CH_4 conversion evolutions for 1% Pt/Cr_2O_3 and 1% Pt/γ-Al_2O_3, respectively. The time on stream behavior of the catalysts during the methane oxidation can be seen from these figures. It is interesting noting that, while, for both catalysts, the methane conversion does not change during the runs, temperatures for obtaining the same CH_4 conversion are higher on 1% Pt/γ-Al_2O_3 than on 1% Pt/Cr_2O_3.

To compare intrinsic catalysts activities of the catalysts, the initial reaction rates (r_0) and the turnover frequencies (TOFs) were calculated from the temporal evolution of CH_4 conversion at 310 °C. The values calculated are presented in Table 2.

For CH_4 oxidation, the TOF value measured at 310 °C on 1% Pt/Cr_2O_3 was about 26 times higher as compared to the TOF value measured on 1% Pt/γ-Al_2O_3 at the same temperature.

The reaction orders on 1% Pt/Cr_2O_3 and on 1% Pt/γ-Al_2O_3 were determined by considering for the initial rate r_0 the following rate equation

$$r_0 = k(P_{CH_4}{}^0)^{\alpha}(P_{O_2}{}^0)^{\beta}$$

where $P_{CH_4}{}^0$ and $P_{O_2}{}^0$ are the partial pressures of CH_4 and O_2, respectively. The effect of $P_{CH4}{}^0$ on kinetic behavior was determined measuring catalytic activities at methane partial pressures between 0.001 and 0.003 atm, while $P_{O_2}{}^0$ was kept constant at 0.1 atm. The effect of $P_{O_2}{}^0$ on kinetic behavior was determined by measuring catalytic activities at oxygen partial pressures between 0.05 and 0.15 atm, while $P_{CH_4}{}^0$ was kept constant at 0.002 atm. Reaction order α was determined from the $\ln(r_0)$ vs $\ln(P_{CH_4}{}^0)$ plot from Figure S9, and the reaction order β was determined from the $\ln(r_0)$ vs $\ln(P_{O_2}{}^0)$ curve from Figure S10. In the figures, it can be seen that the plots can be fitted into straight lines. From the slope of the resulting linear fits, values of $\alpha \cong 1.1$ and $\beta \cong 0$ were determined for 1% Pt/Cr_2O_3 and values of $\alpha \cong 0.9$ and $\beta \cong 0$, for 1% Pt/γ-Al_2O_3 catalyst. The fact that the reaction remains zero order with respect to $P_{O_2}{}^0$ for both catalysts suggests that kinetically relevant C−H bond activation steps occur on surfaces containing species at coverages and reactivities that do not depend on O_2 pressures.

From the ln TOF vs $1/T$ plots (Arrhenius plots) presented in Figure 9, the apparent activation energy (E_a) and the pre-exponential factor A of methane oxidation for the catalysts 1% Pt/Cr_2O_3 and 1% Pt/γ-Al_2O_3 were estimated.

As can be seen in Figure 9, Arrhenius plots for both catalysts can be fitted into straight lines with a correlation coefficient of ~0.99 (least-squares fit). From the slope of the resulting linear fits, the apparent activation energy (E_a) values of 31.85 kcal/mol (1% Pt/Cr_2O_3) and 18.07 kcal/mol (1% Pt/γ-Al_2O_3) could be estimated.

The estimated apparent activation energy of 18.07 kcal/mol is consistent with the values reported previously[7,15,41] for CH_4 oxidation on 1% Pt/γ-Al_2O_3 catalysts. However, the value of 31.86 kcal/mol for the 1% Pt/Cr_2O_3 catalyst is substantially high. This result suggests that the methane oxidation mechanisms on 1% Pt/Cr_2O_3 and 1% Pt/γ-Al_2O_3 are different. The pre-exponential factor associated with 1% Pt/Cr_2O_3 (28.9) is about 12 orders of magnitude larger than that calculated for

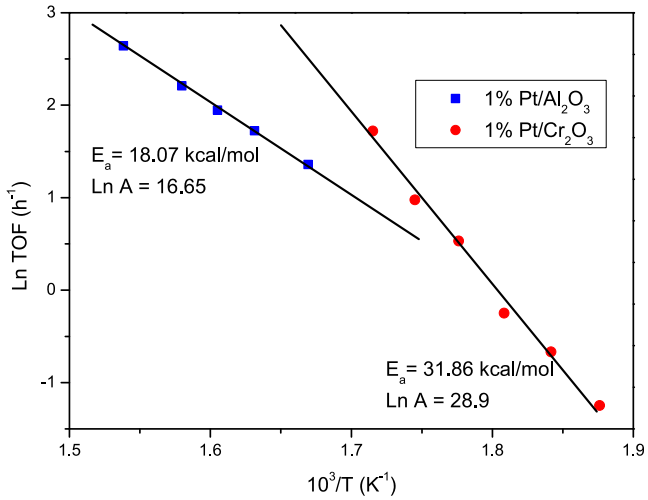

Figure 9. Arrhenius plots (CH_4 oxidation turnover frequency vs $1/T$) utilized to determine the E_a (apparent activation energy) and A (pre-exponential factor) for the 1% Pt/Cr_2O_3 and 1% Pt/γ-Al_2O_3 catalysts in methane oxidation.

1% Pt/γ-Al_2O_3 (16.65). This huge difference can be due to a strong difference in the density of active sites in the two catalysts. Moreover, as the pre-exponential factor is a measure of the frequency of collisions between the reactants and the catalyst surface along with the effectiveness of the orientation of these collisions, the obtained result suggests that the chemical states of the active components in 1% Pt/Cr_2O_3 might have generated a strong energetic field for orientating the collisions in an effective way to increase its effective frequency during methane oxidation reaction. In other words, the active catalytic sites in 1% Pt/Cr_2O_3 might be different in nature and number from the active sites in 1% Pt/γ-Al_2O_3.

3.3. Mechanistic Considerations of CH_4 Oxidation over 1% Pt/Cr_2O_3. The XPS analysis of the 1% Pt/Cr_2O_3 catalyst used for the CH_4 oxidation cycles in this investigation revealed the presence of Pt^0 at its surface despite the high temperature oxidation conditions during catalyst preparation and CH_4 oxidation reactions. As the work function of Pt (6.3 eV) is higher than that of Cr_2O_3 (5.6 eV), an electronic transfer might have occurred at the Pt/Cr_2O_3 interface, increasing the stability of Pt^0 sites, preventing its oxidation to $Pt^{\delta+}$. Moreover, since Cr_2O_3 is an n-type semiconductor, it is capable of transferring electrons to the Pt core, stabilizing the metallic platinum state at the metal−support interface.

On the basis of these facts, we propose a catalytic site model at the catalyst surface, involving Pt^0 sites at the Pt−Cr_2O_3 interface and surface Pt^{x+} (Pt^{4+} or Pt^{2+}) sites in close proximity to Pt^0. Very stable catalytic sites consisting of adjacent Pt^0 and Pt^{x+} (Pt^0−Pt^{x+}) can be developed, which can strongly polarize CH_4 molecules, lowering the C−H bond energy and making the abstraction of the first hydrogen on the adsorbed methane easier by a heterolytic splitting of the C−H bond, following the reaction:

$$(Pt^0{-}Pt^{x+}) + CH_4 \rightarrow (Pt^0)H^+ + (Pt^{x+})CH_3^-$$

Now, the potential of an electric dipole (φ) can be calculated by the relation

$$\varphi = \frac{q_1 - q_2}{4\pi\varepsilon_0 r}$$

DOI: 10.1021/acs.jpcc.8b09748
J. Phys. Chem. C 2019, 123, 2882−2893

Table 4. Electric Dipole Potentials Calculated for the Different Catalytic Sites

	atomic or ionic ratio (r_i) (pm)						
catalytic site	Pt^0	Pt^{2+}	Pt^{4+}	Cr^{3+}	$r\ (r_1 + r_2)$ (pm)	$q_1 - q_2$ (C)	$\varphi(4\pi\varepsilon_0) = (q_1 - q_2)/r$ (C/pm)
Pt^0–Pt^{4+}	177		76.5		253.5	4	0.015
Pt^0–Pt^{2+}	177	94			271	2	0.007
Pt^{2+}–Pt^{4+}		94	76.5		170.5	2	0.011
Pt^0–Cr^{3+}	177			75.5	252.5	3	0.011
Pt^{2+}–Cr^{3+}		94		75.5	169.5	1	0.005
Pt^{4+}–Cr^{3+}			76.5	75.5	152.0	1	0.006

where q_1 and q_2 are the charges corresponding to the first and second ions, respectively, separated by a distance r, and ε_0 is the vacuum permittivity. Considering r as the sum of the radii of the charged species, we have constructed Table 4, listing the values of potentials of the electric dipoles (catalytic sites) which can be generated by the charged species at the surface of the catalyst.

As can be seen in Table 4, the highest electric dipole potential corresponds to Pt^0–Pt^{4+}. Therefore, the probability of CH_4 polarization is highest at this site compared with the polarization probability of CH_4 adsorbed at catalytic (Pt^0–Pt^{2+}), (Pt^{2+}–Pt^{4+}), (Pt^0–Cr^{3+}), (Pt^{2+}–Cr^{3+}), or (Pt^{4+}–Cr^{3+}) sites. These data support the assumption that the presence of Pt^0–Pt^{4+} moieties at the surface is probably the reason for the improved methane oxidation activity of the catalyst. The contribution of the other catalytic sites to the methane oxidation rate cannot be ruled out; however, higher temperatures might be required to attain the activation of the reaction at these sites.

It must be mentioned that, while the formation of Pt ions at the surface of a semiconductor support is driven by the effect of energy alignment between the metal and the semiconductor, the oxidation state of Pt in the catalyst depends also on the particle size of Pt, crystallographic orientation of the support, and preparation conditions of the catalyst.

Now, under the CH_4–O_2 reaction conditions (excess oxygen, 25–600 °C), the platinum surface might be fully covered by oxygen molecules of the reaction atmosphere, preventing CH_4 adsorption. However, CH_4 is adsorbed on Pt^0–Pt^{4+} dipolar sites. In fact, the rate of CH_4 adsorption at the Pt^0–Pt^{4+} dipolar sites would be much higher than that of O_2 due to its nonzero polarizability.[71] On the other hand, as the O_2 molecules are not polarizable (zero polarizability), they remain unaffected by the field generated by Pt^0–Pt^{4+} dipoles. Consequently, the CH_4 molecules will be rapidly attracted to these sites and adsorbed more quickly and strongly than O_2 molecules, as proposed in Figure 10.

This proposed catalytic site model is supported by the values obtained from the kinetic study of the CH_4 oxidation reactions on 1% Pt/Cr_2O_3 and 1% Pt/γ-Al_2O_3. The large difference in the pre-exponential factors in the Arrhenius type equations indicates, on one hand, a large difference between the chemical states of the active sites over 1% Pt/Cr_2O_3 (Pt^0–Pt^{x+}) and 1% Pt/γ-Al_2O_3 (Pt^{2+}) surfaces and, on the other hand, a large difference in frequency and effectiveness of the collisions between the molecules due to their strong orientation induced by the electric dipoles in 1% Pt/Cr_2O_3, which are absent in 1% Pt/γ-Al_2O_3.

In fact, the dipolar model we propose to explain the high catalytic activity of Pt/Cr_2O_3 catalyst for methane oxidation can explain the high activity of Pt catalysts in methane oxidation reported previously,[31,37,41,43] which suggested that an appropriate combination of metallic and oxidic platinum features is

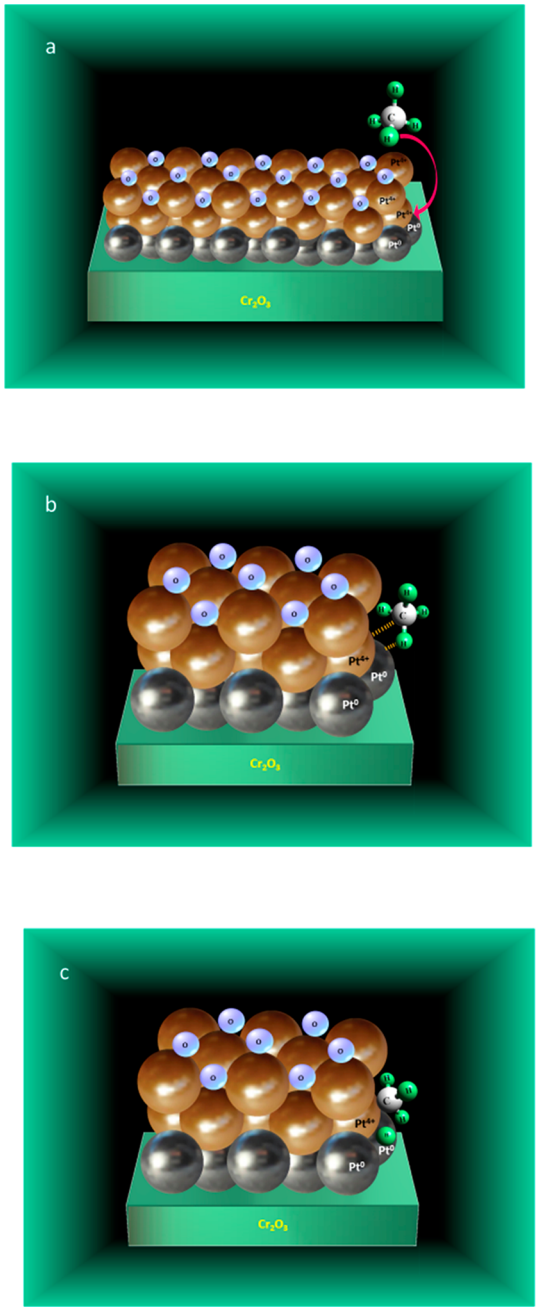

Figure 10. Proposed model for the CH_4 dissociative adsorption over Pt^0–Pt^{4+} dipoles saturated with chemisorbed oxygen atoms: (a) Reactants: CH_4 in the gas phase and 1% Pt/Cr_2O_3; (b) CH_4 polarization by Pt^0–Pt^{4+} site and formation of a transition state; (c) abstraction of the first hydrogen on the adsorbed CH_4 molecule.

DOI: 10.1021/acs.jpcc.8b09748
J. Phys. Chem. C 2019, 123, 2882–2893

the key factor for high activity of platinum catalysts in methane oxidation.

The proposed CH_4 dissociative adsorption mechanism on the Pt^0-Pt^{4+} site is schematically represented in Figure 10.

The subsequent interaction between the adsorbed CH_3^- and H^+ with adsorbed oxygen on the platinum nanoparticle surface would result in the generation of CO_2 and H_2O molecules as final products.

Now, the XPS analysis of the 1% Pt/γ-Al_2O_3 catalyst, fresh and after the CH_4 oxidation cycles, revealed the presence of only Pt^{2+} species at the catalyst surface. The size of the formed particles, determined by TEM of the catalyst, presented an average size of ∼3 nm. It is well-known that small metal nanoparticles can present electron deficiencies due to metal−support interactions.[67,68] This fact and the fact that the catalyst was calcined at 600 °C in air before its use in methane oxidation cycles explain the 100% of Pt^{2+} species present at the catalyst surface. The absence of metallic Pt^0 surface species in 1% Pt/γ-Al_2O_3 as in 1% Pt/Cr_2O_3 can be explained considering the insulating nature of the γ-Al_2O_3. Electronic transfer from γ-Al_2O_3 to Pt does not take place; thus, the metallic state Pt^0 may not be generated and stabilized by electronic transfer. Only Pt^{2+} species are present at the Pt nanoparticles and at the Pt/γ-Al_2O_3 interface, due to the oxidation conditions during catalyst preparation and methane oxidation reaction. At the surface of 1% Pt/γ-Al_2O_3, the formation of a dipolar ($Pt^{\alpha}-Pt^{\beta}$) catalytic site is not probable; thus, the polarization of CH_4 does not take place, preventing the lowering of the C−H bond energy barrier and resulting in very high temperatures for oxidation of CH_4.

It is interesting to note that several previous works have reported the presence of Pt in a zerovalent state (Pt^0) during hydrocarbon oxidation performed over Pt supported metal oxides of non-semiconducting nature.[16,43] As expected, due to the dielectric nature of the support, no electron transfer occurred from the support to the supported Pt to form Pt^0. However, the formation of Pt in different oxidation states depends also on the conditions of catalyst preparation. While Garetto et al.[15] have reported the formation of Pt^0 in their Pt/Al_2O_3 catalyst, which was reduced in pure hydrogen during its preparation, Beck et al.[41] used $Pt(NO_3)_2$ and nitrous acid in different molar ratios for the preparation of Pt/Al_2O_3 catalyst. However, as has been reported by Beck et al.,[41] the ratio of platinum and acid in the precursor solution has a great influence on the mean sizes of the formed Pt particles, which also influences their electronic state. On the other hand, Aryafar et al.[72] reported a kinetic study of the oxidation of alkanes over platinum foil which discards the metal/support interactions in the Pt^0 electronic state.

The results presented in this investigation suggest that the methane oxidation activity of a Pt-supported metal-oxide catalyst can be tuned by controlling the $Pt^{\alpha}-Pt^{\beta}$ dipolar catalytic sites at its surface. The catalytic activity of such dipolar sites depends on the relative values of α and β and on the stability of the electronic state of Pt under Pt−support electronic interactions. The simple preparation method, high activity, low T_{50}, and high stability of the 1% Pt/Cr_2O_3 catalyst for methane oxidation, presented in this study, might lead to its utilization as part of a commercial catalytic converter for lean-burn engines.

CONCLUSIONS

We demonstrated the high methane oxidation capacity of air-calcined 1% Pt/Cr_2O_3 catalyst at low temperature. The results obtained from methane oxidation behavior and electronic state analysis of incorporated platinum in Cr_2O_3 suggest the formation of highly stable Pt^0-Pt^{4+} dipoles at the platinum−support interface, which are highly active catalytic sites for the dissociation and oxidation of methane. These polar catalytic sites promote the abstraction of the first hydrogen of the adsorbed methane molecule, which is the rate-determining step, by a strong polarization of the C−H bonding. The high methane oxidation activity and high stability of the 1% Pt/Cr_2O_3 catalyst presented in this investigation show that the electronic state of platinum and their electronic interactions with the Cr_2O_3 (n-type semiconductor) support surface are the key factors in the methane oxidation process.

ASSOCIATED CONTENT

Supporting Information

The Supporting Information is available free of charge on the ACS Publications website at DOI: 10.1021/acs.jpcc.8b09748.

XPS spectra of Pt $4d_{5/2}$ and Cr $2p_{3/2}$ emissions of 1% Pt/Cr_2O_3; HR-TEM images of 1% Pt/Cr_2O_3; SEM image of Cr_2O_3; methane conversion over 1% Pt/Cr_2O_3 and 1% Pt/Al_2O_3 as a function of time for different reaction temperatures; dependence of methane oxidation rate on CH_4 and O_2 partial pressures for 1% Pt/Cr_2O_3 and 1% Pt/Al_2O_3 used to determine methane and oxygen reaction orders; evolution of temperature of 100% methane conversion (T_{100}) with reaction time over 1% Pt/Cr_2O_3 (PDF)

AUTHOR INFORMATION

Corresponding Author

*E-mail: griselda.corro@correo.buap.mx. Phone: +52 22 2295500-7294.

ORCID

Grisel Corro: 0000-0002-7645-4477

Umapada Pal: 0000-0002-5665-106X

Notes

The authors declare no competing financial interest.

ACKNOWLEDGMENTS

The authors acknowledge Vicerrectoría de Investigación y Estudios de Posgrado, BUAP (Nat 2018-69), and Secretaría de Energía-Consejo Nacional de Ciencia y Tecnología (Cluster Biodiesel 250014), Mexico, for their financial support.

REFERENCES

(1) Mohr, S. H.; Evans, G. M. Long term forecasting of natural gas production. *Energy Policy* **2011**, *39*, 5550−5560.

(2) Munoz, R.; Meier, L.; Diaz, I.; Jeison, D. Rev. A review on the state-of-the-art of physical/chemical and biological technologies for biogas upgrading. *Rev. Environ. Sci. Bio/Technol.* **2015**, *14*, 727−759.

(3) Corro, G.; Pal, U.; Cebada, S. Enhanced biogas production from coffee pulp through deligninocellulosic photocatalytic pretreatment. *Energy Sci. Eng.* **2014**, *2*, 177−187.

(4) Corro, G.; Paniagua, L.; Pal, U.; Bañuelos, F.; Rosas, M. Generation of biogas from coffee-pulp and cow-dung co-digestion: Infrared studies of postcombustion emissions. *Energy Convers. Manage.* **2013**, *74*, 471−481.

(5) Ciuparu, D.; Lyubovsky, M. R.; Altman, E.; Pfefferle, L. D.; Datye, A. Catalytic combustion of methane over palladium-based catalysts. *Catal. Rev.: Sci. Eng.* **2002**, *44*, 593.

(6) Karavalakis, G.; Durbin, T. D.; Villela, M.; Miller, J. W. Air pollutant emissions of light-duty vehicles operating on various natural gas compositions. *J. Nat. Gas Sci. Eng.* **2012**, *4*, 8−16.

DOI: 10.1021/acs.jpcc.8b09748
J. Phys. Chem. C 2019, 123, 2882−2893

(7) Chin, Y.-H.; Buda, C.; Neurock, M.; Iglesia, E. Reactivity of chemisorbed oxygen atoms and their catalytic consequences during CH_4-O_2 catalysis on supported Pt clusters. *J. Am. Chem. Soc.* **2011**, *133*, 15958−15978.
(8) Boucher, O.; Folberth, G. A. New directions: atmospheric methane removal as a way to mitigate climate change. *Atmos. Environ.* **2010**, *44*, 3343−3345.
(9) Carother, F. P.; Schultz, H. L.; Talkington, C. Enviromental Protection Agency: Washington, DC, 2003.
(10) Gelin, P.; Primet, M. Complete oxidation of methane at low temperature over noble metal based catalysts: a review. *Appl. Catal., B* **2002**, *39*, 1−37.
(11) Lin, W.; Zhu, Y. X.; Wu, N. Z.; Xie, Y. C.; Murwani, I.; Kemnitz, E. Total oxidation of methane at low temperature over Pd/TiO_2/Al2O_3: effects of the support and residual chlorine ions. *Appl. Catal., B* **2004**, *50*, 59−66.
(12) Su, S. C.; Carstens, J. N.; Bell, A. T. A study of the dynamics of Pd oxidation and PdO reduction by H_2 and CH_4. *J. Catal.* **1998**, *176*, 125−135.
(13) Persson, K.; Ersson, A.; Jansson, K.; Iverlund, N.; Jaras, S. Influence of co-metals on bimetallic palladium catalysts for methane combustión. *J. Catal.* **2005**, *231*, 139−150.
(14) Abbasi, R.; Wu, L.; Wanke, S. E.; Hayes, R. E. Kinetics of methane combustion over Pt and Pt−Pd catalysts. *Chem. Eng. Res. Des.* **2012**, *90*, 1930−1942.
(15) Garetto, T. F.; Apesteguía, C. R. Oxidative catalytic removal of hydrocarbons over Pt/Al_2O_3 catalysts. *Catal. Today* **2000**, *62*, 189−199.
(16) Liu, W.; Flytzani-Stephanopoulos, M. Total oxidation of carbon monoxide and methane over transition metal-fluorite oxide composite catalysts. *J. Catal.* **1995**, *153*, 304−316.
(17) Zhou, R.; Zhao, B.; Yue, B. Effects of CeO_2-ZrO_2 present in Pd/Al_2O_3 catalysts on the redox behavior of PdO_x and their combustion activity. *Appl. Surf. Sci.* **2008**, *254*, 4701−4707.
(18) Xin, Y.; Wang, H.; Law, C. K. Kinetics of catalytic oxidation of methane, ethane and propane over palladium oxide. *Combust. Flame* **2014**, *161*, 1048−1054.
(19) M'Ramadj, O.; Li, D.; Wang, X.; Zhang, B.; Lu, G. Role of acidity of catalysts on methane combustion over Pd/ZSM-5. *Catal. Commun.* **2007**, *8*, 880−884.
(20) M'Ramadj, O.; Zhang, B.; Li, D.; Wang, X.; Lu, G. Catalytic combustion of methane over high copper-loading ZSM-5 catalysts. *J. Nat. Gas Chem.* **2007**, *16*, 258−265.
(21) Osman, A. I.; Abu-Dahrieh, J. K.; Laffir, F.; Curtin, T.; Thompson, J. M.; Rooney, D. W. A bimetallic catalyst on a dual component support for low temperature total methane oxidation. *Appl. Catal., B* **2016**, *187*, 408−418.
(22) Corro, G.; Cano, C.; Fierro, J. L. G. Promotional effect of C_2−C_4 hydrocarbon on CH_4 oxidation on sulfated Pt/γ-Al_2O_3. *J. Mol. Catal. A: Chem.* **2008**, *281*, 179−183.
(23) Kylhammar, L.; Carlsson, P.-A.; Skoglundh, M. Sulfur promoted low-temperature oxidation of methane over ceria supported platinum catalysts. *J. Catal.* **2011**, *284*, 50−59.
(24) Wilburn, M. S.; Epling, W. S. Sulfur deactivation and regeneration of mono- and bimetallic Pd-Pt methane oxidation catalysts. *Appl. Catal., B* **2017**, *206*, 589−598.
(25) Burch, R.; Urbano, F. J. Investigation of the active state of supported palladium catalysts in the combustion of methane. *Appl. Catal., A* **1995**, *124*, 121−138.
(26) Yoshida, H.; Nakajima, T.; Yazawa, Y.; Hattori, T. Support effect on methane combustion over palladium catalysts. *Appl. Catal., B* **2007**, *71*, 70−79.
(27) Lampert, J. K.; Kazi, M. S.; Farrauto, R. J. Palladium catalyst performance for methane emissions abatement from lean burn natural gas vehicles. *Appl. Catal., B* **1997**, *14*, 211−223.
(28) Hoyos, L. J.; Praliaud, H.; Primet, M. Catalytic combustion of methane over palladium supported on alumina and silica in presence of hydrogen sulfide. *Appl. Catal., A* **1993**, *98*, 125−138.
(29) Gélin, P.; Urfels, L.; Primet, M.; Tena, E. Complete oxidation of methane at low temperature over Pt and Pd catalysts for the abatement of lean-burn natural gas fuelled vehicles emissions: influence of water and sulphur containing compounds. *Catal. Today* **2003**, *83*, 45−57.
(30) Burch, R.; Loader, P. K.; Urbano, F. J. Some aspects of hydrocarbon activation on platinum group metal combustion catalysts. *Catal. Today* **1996**, *27*, 243−248.
(31) Carlsson, P.-A.; Nordström, M.; Skoglundh, M. Virtual Control for High Conversion of Methane Over Supported Pt. *Top. Catal.* **2009**, *52*, 1962.
(32) Carlsson, P.-A.; Fridell, E.; Skoglundh, M. Methane oxidation over Pt/Al2O3 and Pd/Al2O3 catalysts under transient conditions. *Catal. Lett.* **2007**, *115*, 1−7.
(33) Becker, E.; Carlsson, P.-A.; Grönbeck, H.; Skoglundh, M. Methane oxidation over alumina supported platinum investigated by time-resolved in situ XANES spectroscopy. *J. Catal.* **2007**, *252*, 11−17.
(34) Becker, E.; Carlsson, P.-A.; Kylhammar, L.; Newton, M. A.; Skoglundh, M. In situ spectroscopic investigation of low-temperature oxidation of methane over alumina-supported platinum during periodic operation. *J. Phys. Chem. C* **2011**, *115*, 944−951.
(35) Zhdanov, V. P.; Carlsson, P.-A.; Kasemo, B. Simulation of methane oxidation on Pt. *J. Chem. Phys.* **2007**, *126*, 234705.
(36) Burch, R.; Hayes, M. C-H bond activation in hydrocarbon oxidation on solid catalysts. *J. Mol. Catal. A: Chem.* **1995**, *100*, 13.
(37) Burch, R.; Crittle, D. J.; Hayes, M. J. C−H bond activation in hydrocarbon oxidation on heterogeneous catalysts. *Catal. Today* **1999**, *47*, 229−234.
(38) Doornkamp, C.; Ponec, V. The universal character of the Mars and Van Krevelen mechanism. *J. Mol. Catal. A: Chem.* **2000**, *162*, 19−32.
(39) Fujimoto, K.-i.; Ribeiro, F. H.; Avalos-Borja, M.; Iglesia, E. Structure and reactivity of PdOx/ZrO_2 catalysts for methane oxidation at low temperatures. *J. Catal.* **1998**, *179*, 431−442.
(40) Kondo, T.; Yamamoto, T. S. Molecular beam study of CH_4 oxidation on a Pt(111)-(2 × 2)-O Surface. *J. Chem. Phys.* **2003**, *118*, 760.
(41) Beck, I. E.; Bukhtiyarov, V. I.; Pakharukov, I. Y.; Zaikovsky, V. I.; Kriventsov, V. V.; Parmon, V. N. Platinum nanoparticles on Al_2O_3: Correlation between the particle size and activity in total methane oxidation. *J. Catal.* **2009**, *268*, 60−67.
(42) Greiner, M. T.; Helander, M. G.; Tang, W.-M.; Wang, Z.-B.; Qiu, J.; Lu, Z.-H. Universal energy-level alignment of molecules on metal oxides. *Nat. Mater.* **2012**, *11*, 76.
(43) Anderson, J. R. *Structure of Metallic Catalysts*; Academic Press: London, 1975; p 296.
(44) Weckhuysen, B. M.; Wachs, I. E.; Schoonheydt, R. A. Surface chemistry and spectroscopy of chromium in inorganic oxides. *Chem. Rev.* **1996**, *96*, 3327−3350.
(45) Mambrim, J. S. T.; Pastore, H. O.; Davanzo, C. U.; Vichi, E. J. S.; Nakamura, O.; Vargas, H. Synthesis and characterization of chromium silicalite. *Chem. Mater.* **1993**, *5*, 166.
(46) Weckhuysen, B. M.; Schoonheydt, R. A.; Jehng, J. M.; Wachs, I. E.; Cho, S. J.; Ryoo, R.; Kijlstra, S.; Poels, E. Combined DRS-RS-EXAFS-XANES-TPR study of supported chromium catalysts. *J. Chem. Soc., Faraday Trans.* **1995**, *91*, 3245−3253.
(47) Weckhuysen, B. M.; Schoonheydt, R. A.; Mabbs, F. E.; Collison, D. Electron paramagnetic resonance of heterogeneous chromium catalysts. *J. Chem. Soc., Faraday Trans.* **1996**, *92*, 2431−2436.
(48) Weckhuysen, B. M.; Verberckmoes, A. A.; Baets, A. R. D.; Schoonheydt, R. A. Diffuse reflectance spectroscopy of supported chromium oxide catalysts: A self-modeling mixture analysis. *J. Catal.* **1997**, *166*, 160−171.
(49) Mulvaney, P. Surface plasmon spectroscopy of nanosized metal particles. *Langmuir* **1996**, *12*, 788−800.
(50) Wood, A.; Giersig, M.; Mulvaney, P. Fermi level equilibration in quantum dot−metal nanojunctions. *J. Phys. Chem. B* **2001**, *105*, 8810−8815.

DOI: 10.1021/acs.jpcc.8b09748
J. Phys. Chem. C 2019, 123, 2882−2893

(51) Jiang, R.; Li, B.; Fang, C.; Wang, J. Metal/semiconductor hybrid nanostructures for plasmon-enhanced applications. *Adv. Mater.* **2014**, *26*, 5274−5309.
(52) Lietz, G.; Lieske, H.; Spindler, H.; Hanke, W.; Völter, J. Reactions of platinum in oxygen- and hydrogen-treated Ptγ-Al2O3 catalysts: II. Ultraviolet-visible studies, sintering of platinum, and soluble platinum. *J. Catal.* **1983**, *81*, 17−25.
(53) Lieske, H.; Lietz, G.; Spindler, H.; Völter, J. Reactions of platinum in oxygen- and hydrogen-treated Ptγ-Al2O3 catalysts: I. Temperature-programmed reduction, adsorption, and redispersion of platinum. *J. Catal.* **1983**, *81*, 8−16.
(54) Alerasool, S.; Boecker, D.; Rejai, B.; Gonzalez, R.; del Angel, G.; Azomosa, M.; Gomez, R. The role of preparative variables on the surface composition of supported platinum-ruthenium bimetallic clusters. *Langmuir* **1988**, *4*, 1083−1089.
(55) Ma, Y.; Wang, L.; Liu, Z.; Cheng, R.; Zhong, L.; Yang, Y.; He, X.; Fang, Y.; Terano, M.; Liu, B. High-resolution XPS and DFT investigations into Al-modified Phillips CrOx/SiO2 catalysts. *J. Mol. Catal. A: Chem.* **2015**, *401*, 1−12.
(56) Briggs, D., Seah, M. P., Eds. *Practical surface analysis by auger and X-ray photoelectron spectroscopy*, 2nd ed.; Wiley: Chichester, U.K., 1990.
(57) Fang, Y.; Liu, B.; Terano, M. Photo-stability of surface chromate species on Phillips CrO_x/SiO_2 catalysts isothermally calcined at various temperatures, probed by high resolution X-ray photoelectron spectroscopy. *Appl. Catal., A* **2005**, *279*, 131−138.
(58) Drawdy, J. E.; Hoflund, G. B.; Gardner, S. D.; Yngvadottir, E.; Schryer, D. R. Effect of pretreatment on a platinized tin oxide catalyst used for low temperature Co oxidation. *Surf. Interface Anal.* **1990**, *16*, 369−374.
(59) Jackson, S. D.; Willis, J.; McLellan, G. D.; Webb, G.; Keegan, M. B. T.; Moyes, R. B.; et al. Supported metal catalysts: preparation, characterization, and function: I. Preparation and physical characterization of platinum catalysts. *J. Catal.* **1993**, *139*, 191−206.
(60) Kim, K. S.; Winigard, N.; Davis, R. E. Electron spectroscopy of platinum-oxygen surfaces and application to electrochemical studies. *J. Am. Chem. Soc.* **1971**, *93*, 6296−6297.
(61) Arico, A. S.; Shukla, A. K.; Kim, H.; Park, S.; Min, M.; Antonucci, V. An XPS study on oxidation states of Pt and its alloys with Co and Cr and its relevance to electroreduction of oxygen. *Appl. Surf. Sci.* **2001**, *172*, 33−44.
(62) Barr, T. L.; Yin, M. P. Studies of Pt metal catalysis by high-resolution electron microscopy for chemical analysis. Characterization and catalyst development. *ACS Symp. Ser.* **1989**, *411*, 203−213.
(63) Wang, X.; Yu, H.; Hua, D.; Zhou, S. Enhanced catalytic hydrogenation activity and selectivity of Pt-M_xO_y/AL_2O_3 (M = Ni, Fe, Co) heteroaggregate catalysts by in situ transformation of PtM alloy nanoparticles. *J. Phys. Chem. C* **2013**, *117*, 7294−7302.
(64) Escard, J.; Pontvianne, B.; Chenebaux, M. T.; Cosyns, J. *Bull. Soc. Chim. Fr.* **1975**, 2400.
(65) Zsoldos, Z.; Guczi, L. Structure and catalytic activity of alumina supported platinum-cobalt bimetallic catalysts. Effect of treatment on the interface layer. *J. Phys. Chem.* **1992**, *96*, 9393.
(66) Guczi, L.; Sarkany, A.; Koppany, Z. Mechanism of the decomposition of Pt—Co bimetallic particles in NaY zeolites. *Appl. Catal., A* **1994**, *120*, L1−L5.
(67) Ahmadi, M.; Mistry, H.; Roldan Cuenya, B. Tailoring the catalytic properties of metal nanoparticles via support interactions. *J. Phys. Chem. Lett.* **2016**, *7*, 3519−3533.
(68) Cargnello, M.; Doan-Nguyen, V. V. T.; Gordon, T. R.; Diaz, R. E.; Stach, E. A.; Gorte, R. J.; Fornasiero, P.; Murray, C. B. Control of metal nanocrystal size reveals metal-support interface role for ceria. *Science* **2013**, *341*, 771−773.
(69) Cabrera, N.; Mott, N. F. Theory of the oxidation of metals. *Rep. Prog. Phys.* **1949**, *12*, 163.
(70) Gupta, G.; Iqbal, P.; Yin, F.; Liu, J.; Palmer, R. E.; Sharma, S.; Leung, K. C.-F.; Mendes, P. M. Pt diffusion dynamics for the formation Cr−Pt core−shell nanoparticles. *Langmuir* **2015**, *31*, 6917−6923.
(71) Ozier, I. Ground-state electric dipole moment of methane. *Phys. Rev. Lett.* **1971**, *27*, 1329−1335.
(72) Aryafar, M.; Zaera, F. Kinetic study of the catalytic oxidation of alkanes over nickel, palladium, and platinum foils. *Catal. Lett.* **1997**, *48*, 173−183.

DOI: 10.1021/acs.jpcc.8b09748
J. Phys. Chem. C 2019, 123, 2882−2893